Chapter 15

All-Optical Waveguide-Type Switch Using Saturable Absorption in Graphene

Misaki Takahashi, Hiroki Kishikawa,
Nobuo Goto and Shin-ichiro Yanagiya

Additional information is available at the end of the chapter

http://dx.doi.org/10.5772/60437

Abstract

An all-optical switch using saturable absorption that accompanies refractive-index change such as in graphene films is proposed. The switching conditions are theoretically derived for arbitrary values of absorption and refractive-index change. It is found that switching can be performed by weaker control light when the refractive-index change is accompanied in saturable absorption. Switching conditions for various combinations of absorption and refractive-index change are confirmed by FD-BPM simulation. As an experimental demonstration of saturable absorption in graphene, we discuss measured nonlinear absorption in a graphene-loaded waveguide. The saturable absorption and refractive-index change through vertically placed multilayered graphene sheets are also discussed based on reported experimental results.

Keywords: Graphene, integrated optics, optical switch, saturable absorption, nonlinear refractive-index change

1. Introduction

Fast-response optical switches are one of the key devices in photonic routers and in optical signal processors. The switching response depends on the control mechanism of the switch. All-optical switching using optical nonlinear effects has a potential for picosecond-order response. Optically controlled switches include devices using phase shift induced by optical

nonlinear Kerr effect [1] and phase shift in semiconductor optical amplifiers (SOAs) [2] and in quantum dots [3].

We have proposed an all-optical switch controlled by Raman amplification [4,5] or by saturable absorption [6-8], where optical signal amplitude is controlled instead of the signal phase. In the previously proposed switches, refractive-index change induced by all optical nonlinear interactions was assumed to be small enough to be negligible [4,6] or to be adjusted at an integer multiple of 2π [7]. When we assume graphene sheets as the saturable absorbing material, the induced refractive-index change cannot be ignored [9]. In this book chapter, we theoretically analyze the proposed switch to derive switching conditions in general when both the absorption and the index change are induced by nonlinear interaction [8]. It is found that, with arbitrary combination of absorption and induced phase shift, optical switching can be performed by employing appropriate fixed attenuator and fixed phase-shifter in the switching device. We confirm the switching performance by finite-difference beam-propagation-method (FD-BPM) simulation. As an experimental demonstration of saturable absorption in graphene, we also discuss measured nonlinear absorption in a graphene-loaded waveguide [7]. Nonlinear refractive-index change in graphene is also discussed to evaluate optical nonlinear phase change through vertically placed multilayer graphene based on the reported experimental results [9].

2. Graphene for optical processing

Graphene is a two-dimensional (2D) monolayer of sp^2 -bonded carbon atoms and has a dense honeycomb crystal structure. This carbon material has been attracting increasing interest, in particular, since the Nobel Prize was awarded to Novoselov and Geim for their significant contribution in graphene researches [10]. The application areas of graphene are shown in Fig. 1 [11]. Unique characteristics of graphene are driven by its linear massless band structure. In electronic devices, electrons in graphene move at ultrafast speed, and various applications have been investigated. In the field of optics, a monolayer graphene shows large broadband optical absorption of 2.3%, and excellent saturable absorption phenomena having ultrafast carrier dynamics. The saturable absorption has been applied to mode-locked fiber lasers [12-14].

In our proposed optical switch, the saturable absorption characteristics are employed to control optical signal light. In such optical waveguide devices, two schemes, loaded type and vertically inserted type, to introduce graphene in the optical waveguide can be considered as shown in Fig. 2, where graphene is introduced in one of the two arms of a Mach-Zehnder interferometer (MZI) as an example. The former is easy to fabricate in integrated-optic device structure. On the other hand, the latter is easy to evaluate the effect of graphene, whereas optical scattering at the inserted plane of the waveguide may induce insertion loss. We consider all-optical control of signal light by intense control light through saturable absorption.

http://dx.doi.org/10.5772/60437

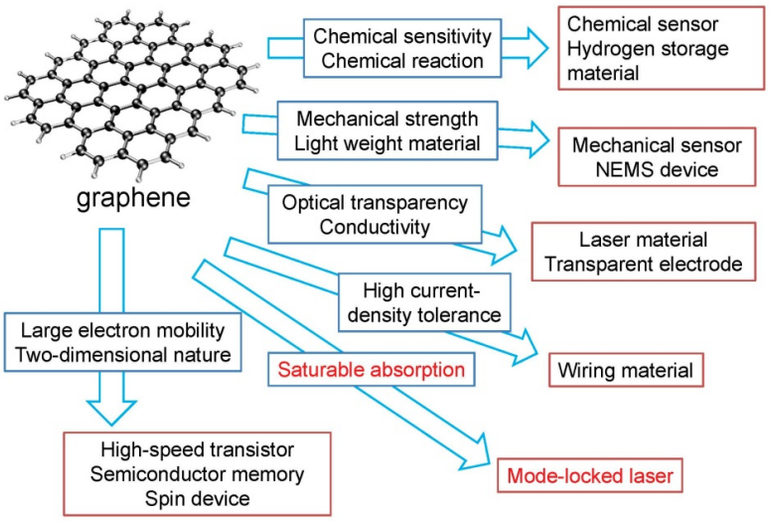

Figure 1. Application area of graphene.

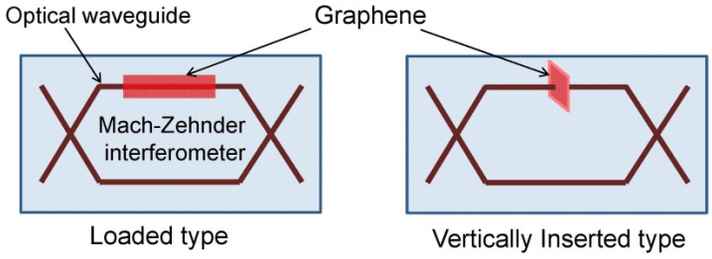

Figure 2. Introduction of graphene in optical waveguide.

We consider a model for controlling the transmittance through a graphene-introduced waveguide. The signal light with electrical-field amplitude $E_{s,in}$ attenuates to be $E_{s,out}$ through the vertically inserted graphene sheets or the graphene-loaded waveguide as shown in Fig. 3(a). The intense control light with electrical-field amplitude $E_{c,in}$ also attenuates to be $E_{c,out}$. The attenuation of the signal light can be decreased by the intense control light due to saturable absorption of graphene. This control of absorption can be equivalently represented by a cascade connection of a fixed attenuator with amplitude attenuation coefficient t_{low} and an amplifier controlled by the control light whose amplitude amplification coefficient is α as shown in Fig. 3(b). The amplification corresponds to decrease of the absorption due to the saturable absorption induced by the intense control light. An induced nonlinear phase shift through saturable absorption is denoted by ϕ. We denote the coefficient including amplification and phase shift as $\alpha' = \alpha \exp(j\ \phi)$. These coefficients are defined by

$$t_{low} = \frac{E_{s,out}(E_{c,in} = 0)}{E_{s,in}}, \tag{1}$$

and

$$\alpha' = \alpha e^{j\phi} = \frac{E_{s,out}(E_{c,in} \neq 0)}{E_{s,out}(E_{c,in} = 0)}. \tag{2}$$

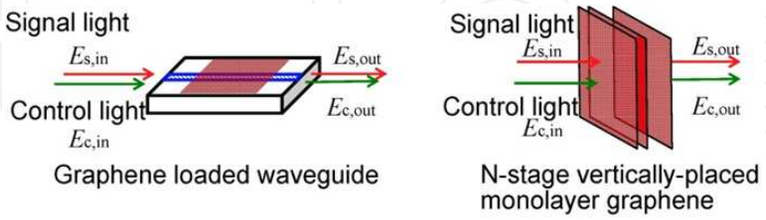

(a)

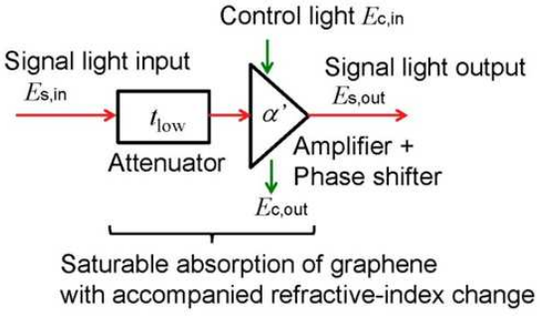

(b)

Figure 3. Modeling of light control by graphene; (a) signal and control lights in graphene, and (b) a model with fixed attenuator and variable amplifier and phase-shifter controlled by control light.

3. Optical switch configuration

The proposed switch consists of two cascaded MZIs connected with asymmetric X-junction couplers, as shown in Fig. 4 [8]. We consider two types of configuration, Type A and B, depending on whether a fixed attenuator is employed in the upper arm of the second MZI or in the lower one, respectively. It is noted that a conventional switch using phase control can be formed with a single MZI. Optical signals in the first MZI are controlled by vertically inserted or overlaid graphene. Control light at a different wavelength or in an orthogonally different polarization from the signal light is coupled in both arms of the first MZI. By inserting the control light, the absorption in the graphene film is reduced due to saturable absorption, which is accompanied by the refractive-index change in the graphene film. Thus, the attenuation and the phase of the signal light along the first MZI arm are controlled by the control light. The transmittance for optical field amplitude in each arm is given by $t_{low}\ \alpha_i \exp(j\phi_i) = t_{low}\ \alpha_i'$, i = A and B. In either arm of the second MZI, a fixed attenuator with a fixed phase-shifter has the transmittance given by $\beta_{fix} = |\beta_{fix}| \exp(j\ \arg(\beta_{fix}))$.

http://dx.doi.org/10.5772/60437

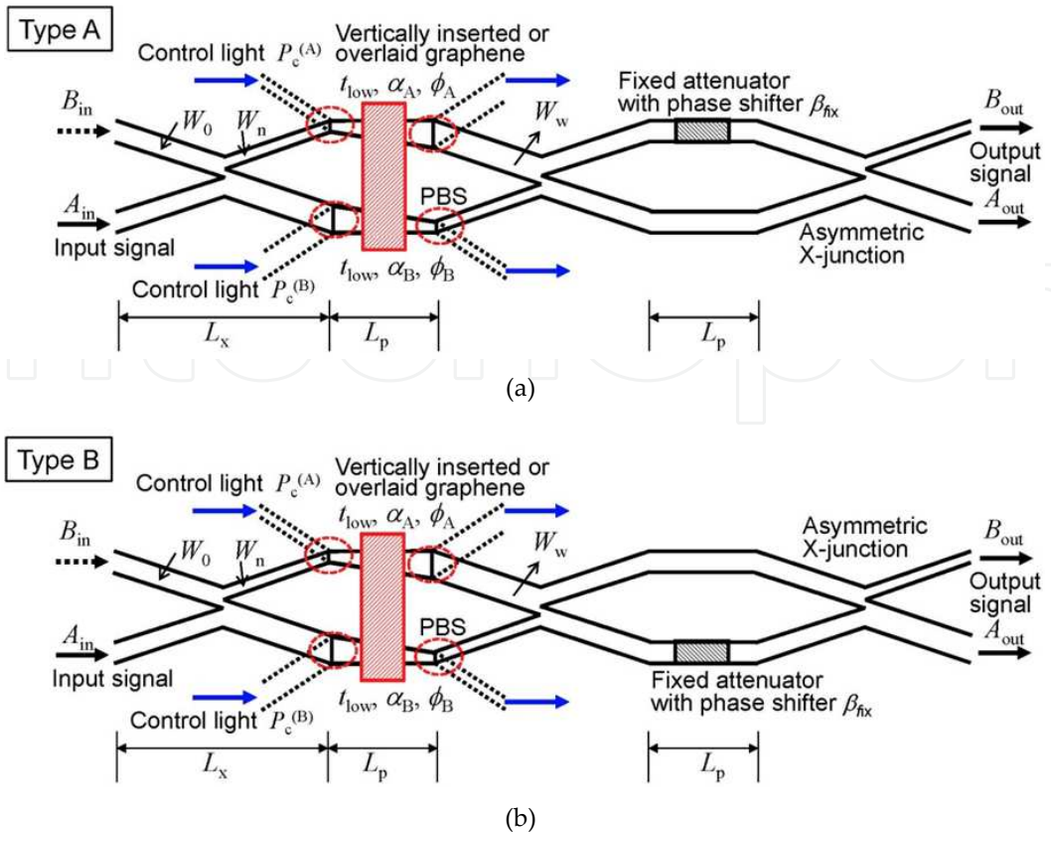

Figure 4. Switch structure; (a) Type A and (b) Type B.

Switching response time is mainly limited by the response of the saturable absorption in graphene. It is reported that, from pump-probe experiments, the carrier relaxation time and carrier–carrier intraband scattering time-constant are less than 1 ps [13]. A response time in a 20-μm-long graphene-coated microfiber was also measured to be 2.2 ps [15]. Since the switching is kept as on-state during the control signal existence, optical control pulse with rise and fall time less than 1 ps can result in picosecond switching.

4. Switching conditions

The input-to-output relation for optical field amplitudes in case of Type A shown in Fig. 4(a) is given by

$$\begin{bmatrix} A_{out} \\ B_{out} \end{bmatrix} = \left(\frac{1}{\sqrt{2}}\right)^3 \begin{bmatrix} 1 & 1 \\ -1 & 1 \end{bmatrix} \begin{bmatrix} 1 & 0 \\ 0 & \beta_{fix} \end{bmatrix} \begin{bmatrix} 1 & 1 \\ -1 & 1 \end{bmatrix} \begin{bmatrix} t_{low}\alpha_B' & 0 \\ 0 & t_{low}\alpha_A' \end{bmatrix} \begin{bmatrix} 1 & 1 \\ -1 & 1 \end{bmatrix} \begin{bmatrix} A_{in} \\ B_{in} \end{bmatrix}$$
$$= \frac{t_{low}}{2\sqrt{2}} \begin{bmatrix} a_{11} & a_{12} \\ a_{21} & a_{22} \end{bmatrix} \begin{bmatrix} A_{in} \\ B_{in} \end{bmatrix} \quad (3)$$

where

$$\begin{cases} a_{11} = \alpha_A^{'} - \alpha_B^{'} - \beta_{\text{fix}}(\alpha_A^{'} + \alpha_B^{'}) \\ a_{12} = \alpha_A^{'} + \alpha_B^{'} + \beta_{\text{fix}}(-\alpha_A^{'} + \alpha_B^{'}) \\ a_{21} = -\alpha_A^{'} + \alpha_B^{'} - \beta_{\text{fix}}(\alpha_A^{'} + \alpha_B^{'}) \\ a_{22} = -\alpha_A^{'} - \alpha_B^{'} + \beta_{\text{fix}}(-\alpha_A^{'} + \alpha_B^{'}) \end{cases}. \tag{4}$$

Similar equations for input-to-output relation in Type B shown in Fig. 4(b) are derived as

$$\begin{aligned} \begin{bmatrix} A_{\text{out}} \\ B_{\text{out}} \end{bmatrix} &= \left(\frac{1}{\sqrt{2}}\right)^3 \begin{bmatrix} 1 & 1 \\ -1 & 1 \end{bmatrix} \begin{bmatrix} \beta_{\text{fix}} & 0 \\ 0 & 1 \end{bmatrix} \begin{bmatrix} 1 & 1 \\ -1 & 1 \end{bmatrix} \begin{bmatrix} t_{\text{low}}\alpha_B^{'} & 0 \\ 0 & t_{\text{low}}\alpha_A^{'} \end{bmatrix} \begin{bmatrix} 1 & 1 \\ -1 & 1 \end{bmatrix} \begin{bmatrix} A_{\text{in}} \\ B_{\text{in}} \end{bmatrix} \\ &= \frac{t_{\text{low}}}{2\sqrt{2}} \begin{bmatrix} a_{11} & a_{12} \\ a_{21} & a_{22} \end{bmatrix} \begin{bmatrix} A_{\text{in}} \\ B_{\text{in}} \end{bmatrix} \end{aligned} \tag{5}$$

where

$$\begin{cases} a_{11} = -\alpha_A^{'} - \alpha_B^{'} + \beta_{\text{fix}}(\alpha_A^{'} - \alpha_B^{'}) \\ a_{12} = -\alpha_A^{'} + \alpha_B^{'} + \beta_{\text{fix}}(\alpha_A^{'} + \alpha_B^{'}) \\ a_{21} = -\alpha_A^{'} - \alpha_B^{'} - \beta_{\text{fix}}(\alpha_A^{'} - \alpha_B^{'}) \\ a_{22} = -\alpha_A^{'} + \alpha_B^{'} - \beta_{\text{fix}}(\alpha_A^{'} + \alpha_B^{'}) \end{cases}. \tag{6}$$

We consider the case that an optical signal is incident only at the lower port, that is, $A_{\text{in}}=E_{\text{in}}$ and $B_{\text{in}}=0$. Then, eqs. (3) and (5) are simplified to be

$$\begin{bmatrix} A_{\text{out}} \\ B_{\text{out}} \end{bmatrix} = \frac{t_{\text{low}}E_{\text{in}}}{2\sqrt{2}} \begin{bmatrix} a_{11} \\ a_{21} \end{bmatrix}. \tag{7}$$

We now derive the conditions required for complete switching. We assume that switching is operated by feeding a control light with power $P_c^{(A)}$ in the upper arm of the first MZI to switch to the lower output port as A_{out}, and by feeding a control light $P_c^{(B)}$ in the lower arm to switch to the upper output port as B_{out}. Therefore, the parameters $\alpha_A^{'}$ and $\alpha_B^{'}$ due to saturable absorption are to be set as $\alpha_A^{'}=1$ to switch to the upper output port as B_{out} and $\alpha_B^{'}=1$ to switch to the lower output port as A_{out} because no control light is fed in these arms.

Switching conditions for β_{fix} and the output field B_{out} in the case of Type A are obtained from eqs. (4) and (7) as follows:

1. Switching to B_{out} :

$$\beta_{\text{fix}} = \frac{\alpha_B^{'} - 1}{\alpha_B^{'} + 1} \text{ and } B_{\text{out}} = \frac{t_{\text{low}} E_{\text{in}} (1 - \alpha_B^{'})}{\sqrt{2}}. \tag{8}$$

2. Switching to A_{out} :

$$\beta_{\text{fix}} = \frac{\alpha_A^{'} - 1}{\alpha_A^{'} + 1} \text{ and } A_{\text{out}} = \frac{t_{\text{low}} E_{\text{in}} (1 - \alpha_A^{'})}{\sqrt{2}}. \tag{9}$$

It is found from these conditions that, when $\alpha_A^{'}$ for switching to A_{out} is equal to $\alpha_B^{'}$ for switching to B_{out}, switching can be operated with a fixed β_{fix}.

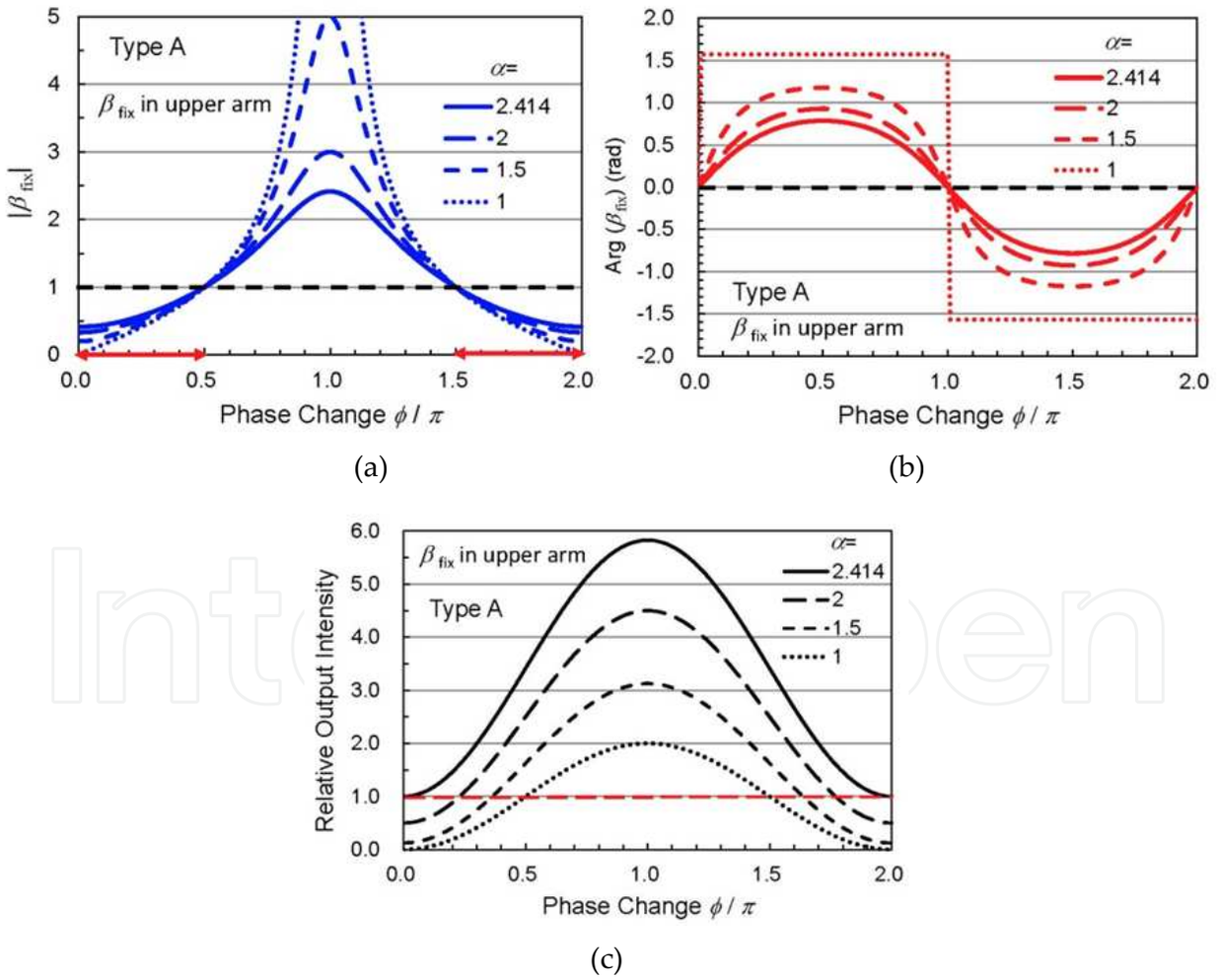

Figure 5. Switching conditions in switch Type A; (a) the fixed attenuator and (b) phase-shifter in the second MZI required for switching and (c) the output intensity.

Similarly, switching conditions in the case of Type B are obtained from eqs. (6) and (7) as follows:

1. Switching to B_{out} :

$$\beta_{\text{fix}} = \frac{\alpha_B^{'} + 1}{\alpha_B^{'} - 1} \text{ and } B_{\text{out}} = -\frac{t_{\text{low}} E_{\text{in}} (1 + \alpha_B^{'})}{\sqrt{2}}. \tag{10}$$

2. Switching to A_{out} :

$$\beta_{\text{fix}} = \frac{\alpha_A^{'} + 1}{\alpha_A^{'} - 1} \text{ and } A_{\text{out}} = \frac{t_{\text{low}} E_{\text{in}} (1 + \alpha_A^{'})}{\sqrt{2}}. \tag{11}$$

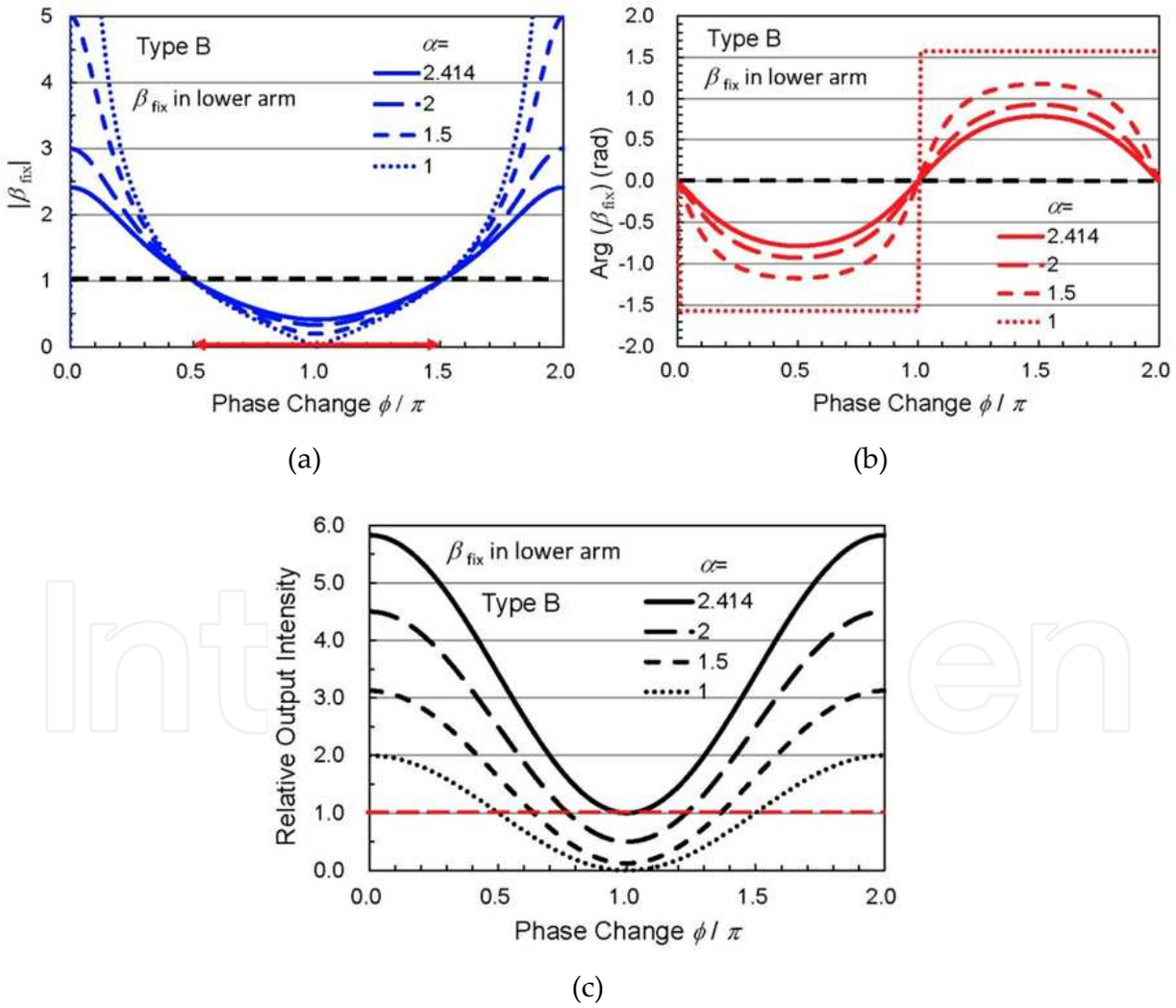

Figure 6. Switching conditions in switch Type B; (a) the fixed attenuator and (b) phase-shifter in the second MZI required for switching and (c) the output intensity.

From these equations, switching conditions required for β_{fix} and the relative output intensities $|A_{\mathrm{out}}/(t_{\mathrm{low}}E_{\mathrm{in}})|^2$ and $|B_{\mathrm{out}}/(t_{\mathrm{low}}E_{\mathrm{in}})|^2$ are calculated as a function of phase change ϕ_{A} or ϕ_{B} as shown in Figs. 5 and 6 for Type A and B, respectively, where $\alpha_i=1+\sqrt{2}$, 2.0, 1.5, and 1.0 are assumed as a parameter. Since $|\beta_{\mathrm{fix}}|\leq 1$ can be realized by an attenuator, Type A should be selected for $|\phi_i|\leq\pi/2$ and $3\pi/2\leq|\phi_i|\leq 2\pi$ and Type B for $\pi/2\leq|\phi_i|\leq 3\pi/2$, respectively, in the range of $0\leq|\phi_i|\leq 2\pi$. An arbitrary combination of α_i and ϕ_i can be used to operate switching by adjusting $|\beta_{\mathrm{fix}}|$ and $\arg(\beta_{\mathrm{fix}})$.

We consider three cases as examples of switching. As a first case, case (1), we assume that no phase shift is accompanied in saturable absorption, that is, $\phi_A=\phi_B=0$, and no phase shift is set in β_{fix}. This corresponds to the case discussed in ref. [7]. The switching conditions in Type A are derived from eqs. (8) and (9) as follows:

1. Switching to B_{out} ($\alpha_A'=1,\ \alpha_B'=1+\sqrt{2}$) :

$$\beta_{\mathrm{fix}}=\frac{1}{1+\sqrt{2}}\left(\rightarrow\arg\left(\beta_{\mathrm{fix}}\right)=0\right)\ \text{and}\ B_{\mathrm{out}}=-t_{\mathrm{low}}E_{\mathrm{in}}. \tag{12}$$

2. Switching to A_{out} ($\alpha_A'=1+\sqrt{2},\ \alpha_B'=1$) :

$$\beta_{\mathrm{fix}}=\frac{1}{1+\sqrt{2}}\left(\rightarrow\arg\left(\beta_{\mathrm{fix}}\right)=0\right)\ \text{and}\ A_{\mathrm{out}}=-t_{\mathrm{low}}E_{\mathrm{in}}. \tag{13}$$

This case corresponds to $\alpha_i=1+\sqrt{2}\cong 2.414$ and $\phi_i=0$ in Fig. 5(a). The operating point for β_{fix} and the output intensity are indicated by red circles on green curves in Fig. 7(a).

As a next case, case (2a), we assume the same $\alpha_i=1+\sqrt{2}$ as case (1), whereas a phase shift $\phi_i=\pi/2$ is accompanied. The switching conditions in Type A are derived from eqs. (8) and (9) as follows:

1. Switching to B_{out} ($\alpha_A'=1,\ \alpha_B=1+\sqrt{2},\ \phi_B=\pi/2$) :

$$\beta_{\mathrm{fix}}=\frac{j\left(1+\sqrt{2}\right)-1}{j\left(1+\sqrt{2}\right)+1}\left(\rightarrow\left|\beta_{\mathrm{fix}}\right|=1,\arg\left(\beta_{\mathrm{fix}}\right)=\frac{\pi}{4}\right)\ \text{and}\ B_{\mathrm{out}}=\frac{t_{\mathrm{low}}E_{\mathrm{in}}[1-j\left(1+\sqrt{2}\right)]}{\sqrt{2}}. \tag{14}$$

2. Switching to A_{out} ($\alpha_A=1+\sqrt{2},\ \phi_A=\pi/2,\ \alpha_B'=1$) :

$$\beta_{\mathrm{fix}}=\frac{j\left(1+\sqrt{2}\right)-1}{j\left(1+\sqrt{2}\right)+1}\left(\rightarrow\left|\beta_{\mathrm{fix}}\right|=1,\arg\left(\beta_{\mathrm{fix}}\right)=\frac{\pi}{4}\right)\ \text{and}\ A_{\mathrm{out}}=\frac{t_{\mathrm{low}}E_{\mathrm{in}}[1-j\left(1+\sqrt{2}\right)]}{\sqrt{2}}. \tag{15}$$

It is noted that, since $\{[1-j(1+\sqrt{2})]/\sqrt{2}\}^2=2+\sqrt{2}$, the output intensity is increased from 1.0 to 3.41 compared with case(1). Thus, when $\phi_i=\pi/2$ is accompanied in saturable absorption, the excess

loss through the switch is decreased by $10\log_{10}(2+\sqrt{2})=5.33$ (dB). The operating point for β_{fix} and the output intensity are indicated in Fig. 7(b).

When ϕ_i increases further to $\pi/2 \le \phi_i \le 3\pi/2$, switching in type A cannot be realized with a fixed attenuator because $|\beta_{\text{fix}}| \ge 1$, and the switch structure of Type B has to be used to realize with a fixed attenuator. In this case, $|\beta_{\text{fix}}|$, $\arg(\beta_{\text{fix}})$ and the normalized output are found in Fig. 6. We consider a case of $\phi_i=\pi$ as case (2b). The switching conditions in Type B are derived from eqs. (10) and (11) as follows:

1. Switching to B_{out} ($\alpha_A'=1,\ \alpha_B=1+\sqrt{2},\ \phi_B=\pi$) :

$$\beta_{\text{fix}}=\frac{1}{1+\sqrt{2}}\left(\rightarrow \arg\left(\beta_{\text{fix}}\right)=0\right) \text{ and } B_{\text{out}}=t_{\text{low}}E_{\text{in}}. \tag{16}$$

2. Switching to A_{out} ($\alpha_A=1+\sqrt{2},\ \phi_A=\pi,\ \alpha_B'=1$) :

$$\beta_{\text{fix}}=\frac{1}{1+\sqrt{2}}\left(\rightarrow \arg\left(\beta_{\text{fix}}\right)=0\right) \text{ and } A_{\text{out}}=t_{\text{low}}E_{\text{in}}. \tag{17}$$

The same switching conditions are found for $\phi_i=(2n-1)\pi$, $n=1, 2, \ldots$. It is noted that, for $\phi_i=2n\pi$, the same switching conditions as for $\phi_i=0$ in Type A are applied. The operating point for β_{fix} and the output intensity are indicated in Fig. 7(c).

We consider improvement of control efficiency by taking the phase shift ϕ_i and $\arg(\beta_{\text{fix}})$ into account. Although $\alpha_i=1+\sqrt{2}$ is required with a fixed β_{fix} with $\arg(\beta_{\text{fix}})=0$ in the second MZI, switching can be performed even with $\alpha_i<1+\sqrt{2}$ as shown in Figs. 5 and 6. We consider a case of $\phi_i=0$. By decreasing α_i from $1+\sqrt{2}$ to 2.0, the required β_{fix} decreases to $1/3$, resulting in decrease of the normalized output from 1 to 1/2 as shown in Fig. 5. Thus, by decreasing α_i from $1+\sqrt{2}$ to 2.0, insertion loss of the switch increases by 3 dB. Next, we consider a case of $\phi_i=\pi/2$ and $\alpha_i=2.0$ as case(3). The switching conditions in Type A are derived from eqs. (8) and (9) as follows:

1. Switching to B_{out} ($\alpha_A'=1,\ \alpha_B=2,\ \phi_B=\pi/2$) :

$$\beta_{\text{fix}}=\frac{3+j4}{5}\left(\rightarrow |\beta_{\text{fix}}|=1,\ \arg\left(\beta_{\text{fix}}\right)=0.927\right) \text{ and } B_{\text{out}}=\frac{t_{\text{low}}E_{\text{in}}(1-j2)}{\sqrt{2}}. \tag{18}$$

2. Switching to A_{out} ($\alpha_A=2,\ \phi_A=\pi/2,\ \alpha_B'=1$) :

$$\beta_{\text{fix}}=\frac{3+j4}{5}\left(\rightarrow \left|\beta_{\text{fix}}\right|=1, \arg\left(\beta_{\text{fix}}\right)=0.927\right) \text{ and } A_{\text{out}}=\frac{t_{\text{low}}E_{\text{in}}(1-j2)}{\sqrt{2}}. \tag{19}$$

http://dx.doi.org/10.5772/60437

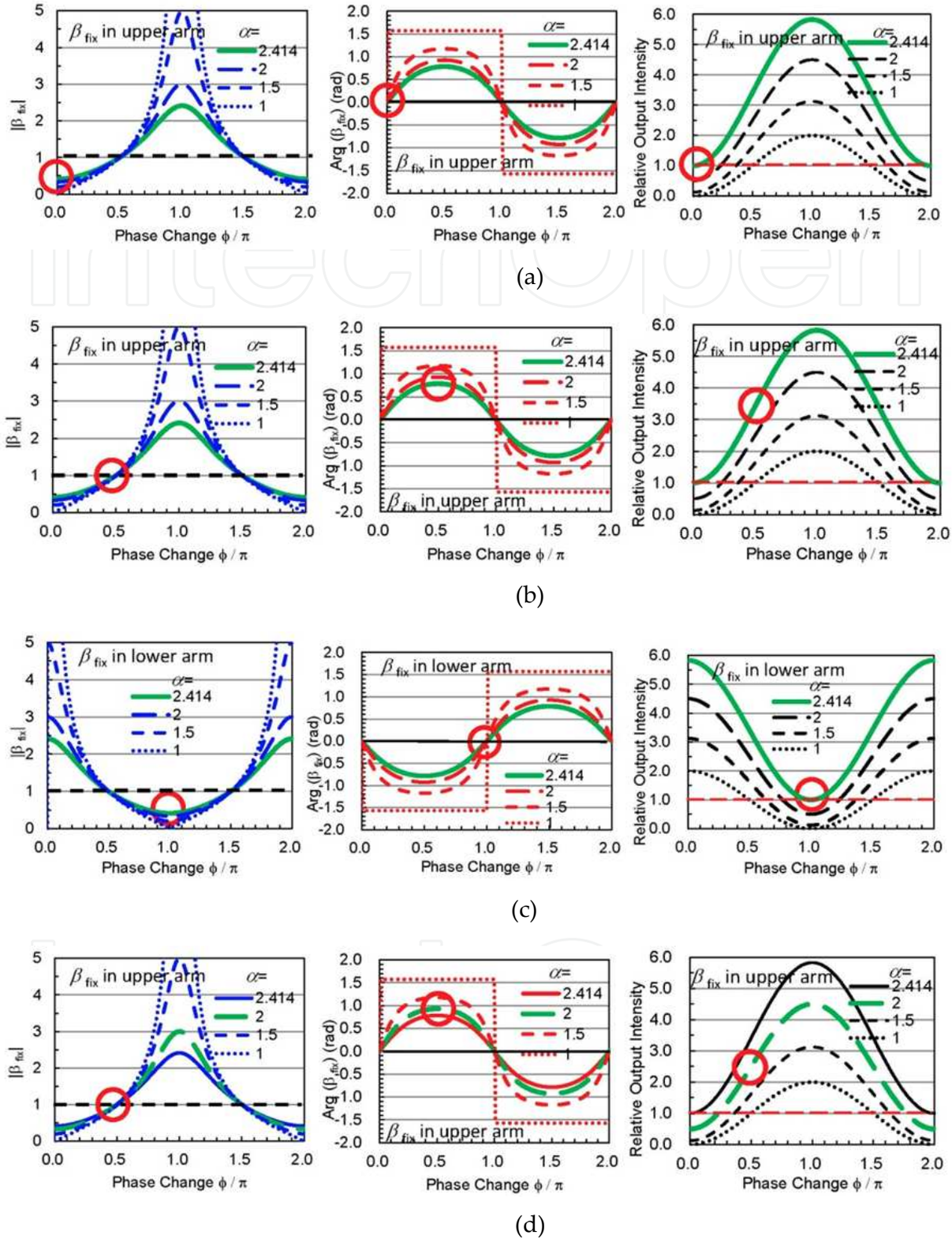

Figure 7. Operation points in the switching conditions for four kinds of switches: (a) case(1), (b) case(2a), (c) case(2b), and (d) case(3).

Since $[(1-j2)/\sqrt{2}]^2=2.5$, the output intensity is increased by 2.5 times compared with case(1). The operating point for β_{fix} and the output intensity are indicated in Fig. 7(d). In the case with a further reduced α_i, switching can be operated by employing appropriate fixed $|\beta_{\text{fix}}|$ and $\arg(\beta_{\text{fix}})$ according to the phase shift ϕ_i.

Finally, we consider a limited case with $\alpha_i=1.0$, that is, no saturable absorption is used but the phase shift ϕ_i alone is used in switching. When ϕ_i is increased to $\pi/2$, β_{fix} is derived to be $\beta_{\text{fix}}=(-1+j)/(1+j)=e^{j\pi/2}$, that is, a $\pi/2$ phase-shifter is used as β_{fix}. The normalized output intensity is 1.0. When ϕ_i is further increased to π, $|\beta_{\text{fix}}|$ reduced to 0 in Type B. No output is obtained in this case. This switching condition of $\phi_i=\pi$ is used in a conventional switch consisting of a single MZI. That is, the switching is performed at the output of the first MZI. Since β_{fix} is designed to equalize the optical intensity in the two arms of the second MZI, switching cannot be performed with the proposed two-stage MZI switch, for $\alpha_i=1.0$ and $\phi_i=\pi$.

5. FD-BPM simulation

In order to confirm the switching operation with the proposed switch, FD-BPM simulation was performed under various switching conditions. We consider a 2D slab waveguide model. The core and cladding regions have refractive indices of $n_c = 1.461$ and $n_s = 1.45$, respectively. The waveguide widths of the fundamental, narrow, and wide waveguides of the asymmetric X-junctions are $W_1=3.0$ μm, $W_n=2.6$ μm, and $W_w=3.4$ μm, respectively. Optical waves are assumed to be TE mode. The lengths of the X-junction coupler and the parallel waveguides in arms are L_x =16 mm and L_p =1 mm, respectively. The total length is 50 mm. The distance of the two input ports is 23 μm. The optical wavelength is 1550 nm.

In the simulation, α_i and ϕ_i caused by saturable absorption are equivalently simulated just by multiplying the optical electric field by the coefficient $\alpha_i e^{j\phi_i}$ at a plane located at the end of the graphene-loaded or graphene-inserted waveguide. The waveguides for coupling the control light are not modeled in this simulation. In a similar manner, the attenuation corresponding to t_{low}, the fixed attenuator and the phase-shifter β_{fix} are modeled by multiplying the optical electric field by t_{low} and $|\beta_{\text{fix}}|\exp[j\ \arg(\beta_{\text{fix}})]$, respectively. The value of t_{low} is assumed to be an ideal value of $1/(1+\sqrt{2})$, where the optical signal does not attenuate through graphene with intense control light.

Fig. 8(a) shows optical intensities along the switch in case (1) obtained by FD-BPM simulation, where $\alpha_i=1+\sqrt{2}$, $\phi_i=0$, and $\beta_{fix}=1/(1+\sqrt{2})$ are assumed. Similarly, optical intensities along the switch in case (2a), case (2b), and case (3) are plotted in Fig. 8(b), (c), and (d), respectively. The switched output intensities are summarized in Table 1. The simulated outputs show good agreement with theoretical results with error less than 3.5%.

http://dx.doi.org/10.5772/60437

6. Measurement of saturable absorption through graphene-loaded waveguide

In this section, we show an experimental result of optical saturable absorption in a monolayer-graphene-loaded waveguide. The optical waveguide was fabricated by K^+ ion exchange on a soda-lime glass substrate. Optical waveguide was formed by K^+ ion exchange through a 30 μm opening in an aluminum mask. Potassium nitrate was used as the ion source and ion exchange was carried out at 370 degrees Celsius for 4 hours. After polishing the end facets of the waveguide, a sheet of monolayer graphene was transferred on the glass substrate surface. The monolayer graphene was formed by CVD on copper foil (iTRIX Corporation). The length of the graphene sheet is about 7 mm. The waveguide structure is shown in Fig. 9(a). A microscopic top-view of the waveguide and a near-field output intensity profile from the waveguide output end facet are also shown in Fig. 9(b) and (c), respectively. Raman spectrum of the transferred graphene on the glass substrate was measured as shown in Fig. 10. In the Raman spectrum, the D peak at 1350 cm^{-1} is correlated with the disorder of the graphene lattice; the G peak at 1580 cm^{-1} and the 2D peak around 2700 cm^{-1} correspond to the phonon excitation at the Brillouin zone center and the second-order of zone-boundary phonons, respectively [16].

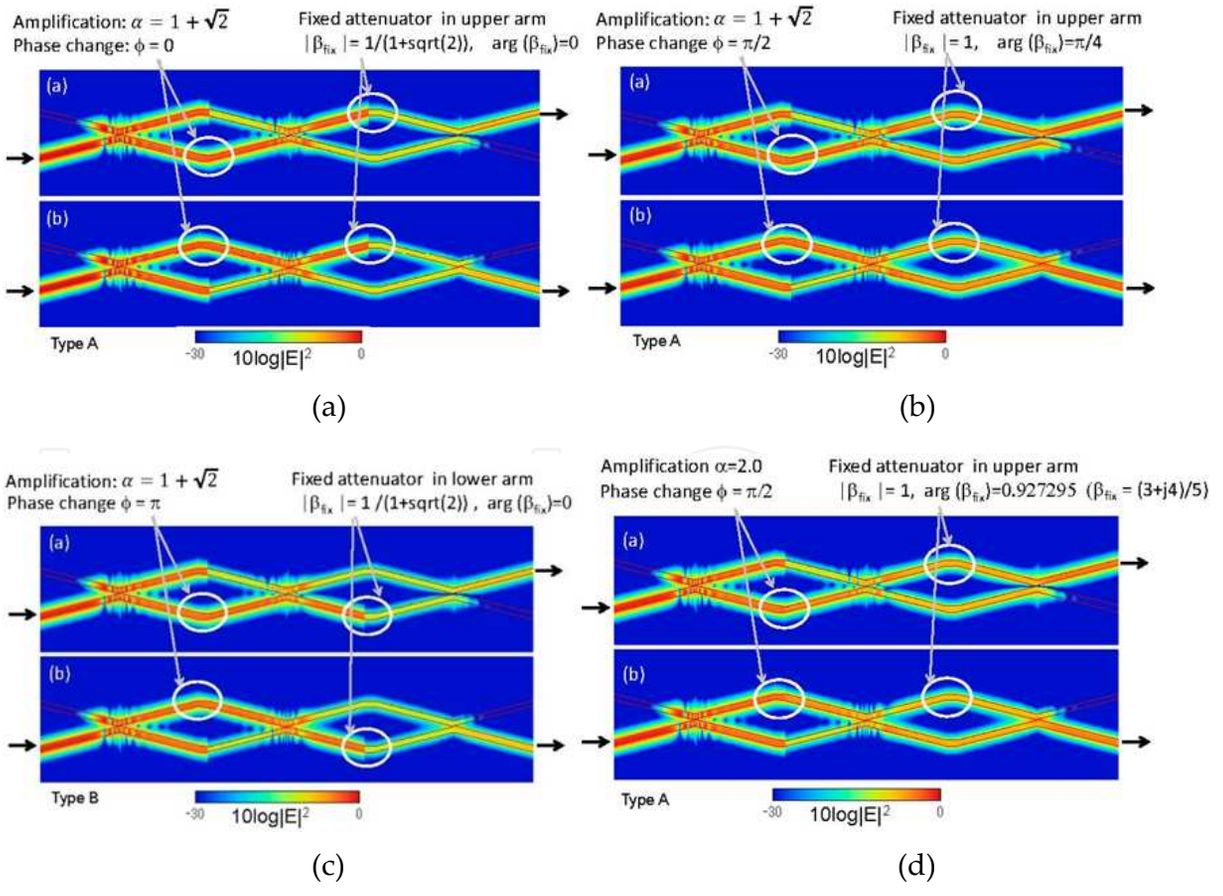

Figure 8. Optical signal intensities along the switches obtained by FD-BPM simulation for (a) case(1), (b) case(2a), (c) case(2b), and (d) case(3).

Case	α_i	ϕ_i	$\lvert\beta_{fix}\rvert$	$\arg(\beta_{fix})$	Control arm	Theory		Simulation	
						$\lvert A_{out}\rvert^2$	$\lvert B_{out}\rvert^2$	$\lvert A_{out}\rvert^2$	$\lvert B_{out}\rvert^2$
(1)	$1+\sqrt{2}$	0	$\frac{1}{1+\sqrt{2}}$	0	B	0	0.1716	6.281×10^{-4}	1.653×10^{-1}
					A	0.1716	0	1.689×10^{-1}	6.195×10^{-4}
(2a)	$1+\sqrt{2}$	$\frac{\pi}{2}$	1	$\frac{\pi}{4}$	B	0	0.5858	1.197×10^{-3}	5.647×10^{-1}
					A	0.5858	0	5.704×10^{-1}	1.168×10^{-3}
(2b)	$1+\sqrt{2}$	π	$\frac{1}{1+\sqrt{2}}$	0	B	0	0.1716	6.158×10^{-4}	1.665×10^{-1}
					A	0.1716	0	1.680×10^{-1}	6.060×10^{-4}
(3)	2	$\frac{\pi}{2}$	1	$\arg\left(\frac{3+j4}{5}\right)$	B	0	0.4289	1.101×10^{-3}	4.135×10^{-1}
					A	0.4289	0	4.173×10^{-1}	1.070×10^{-3}

Table 1. Theoretical and simulated output intensities.

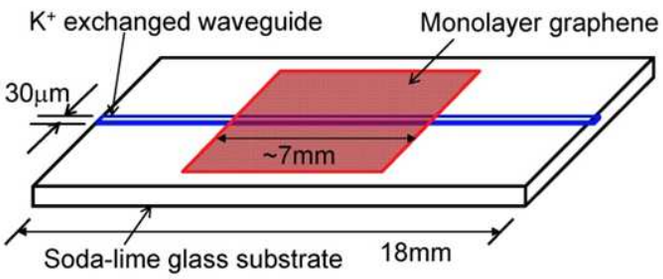

(a)

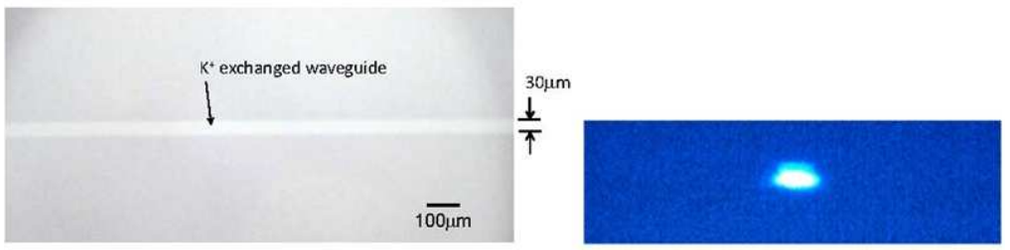

(b) (c)

Figure 9. Graphene-loaded optical waveguide; (a) the structure, (b) the microscopic top-view, and (c) the near field pattern from the waveguide.

The experimental setup for measuring saturable absorption is illustrated in Fig. 11. A 1.56 μm femtosecond laser with width of 0.4 ps at repetition rate of 41.96 MHz was used as the laser source. The average power is 4.4 mW. The polarization-controlled laser light was coupled into the waveguide by ×20 objective lens.

Figure 12 shows the measured insertion loss for TE and TM modes as a function of the incident average power at the waveguide input. The measured loss includes coupling loss, waveguide-propagation loss and attenuation loss due to graphene. The insertion loss reduces by more than 10 dB as the incident power increases. This is considered to be caused by saturable

http://dx.doi.org/10.5772/60437

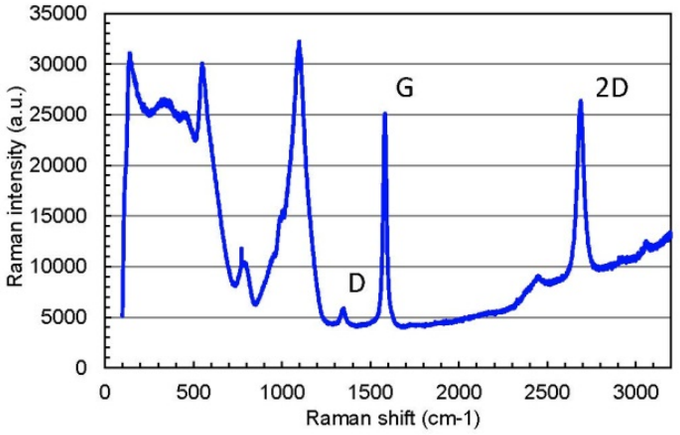

Figure 10. Raman spectrum from the graphene-loaded waveguide.

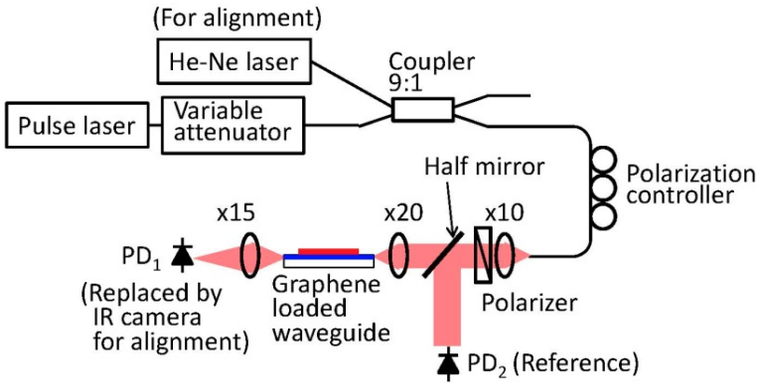

Figure 11. Experimental setup for measurement of nonlinear insertion loss.

absorption of graphene. This modulation depth of the transmittance through the waveguide satisfies the requirement for optical switching. The insertion loss in TM mode is larger than that in TE mode by about 10 dB at low optical power. The difference reduces to about 3dB at high optical power.

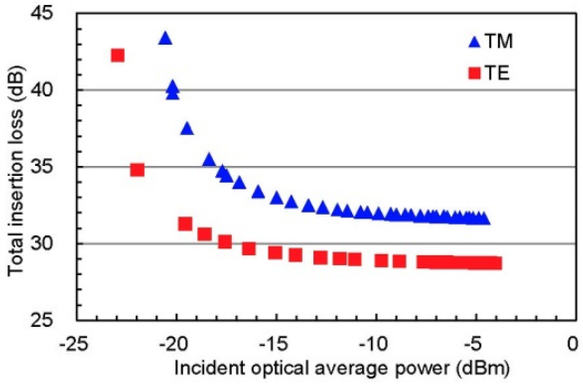

Figure 12. Nonlinear insertion loss through a graphene-loaded optical waveguide.

7. Evaluation of transmittance and phase shift in loosely multilayered graphene

It is found from the discussion in the previous sections that the switch can be operated by adjusting the fixed β_{fix} in the second MZI even if the phase shift ϕ_i is unknown. In this section, we discuss the transmittance and the phase shift in vertically inserted multilayered graphene based on a reported experimental result by H. Zhang et al. [9]. The transmittance in loosely stacked three-layer graphene was measured and was reported to be fitted by the following experimental formula:

$$T(I) = T(0) + \Delta T_0 - \frac{\Delta T_0}{1 + I / I_{\text{sat}}} \tag{20}$$

where I is the incident optical peak power density, $T(0)$ is the transmittance at weak optical power density. The parameters fitted with the experimental data are ΔT_0=0.051, I_{sat}=0.074 GW/cm^2. When $T(0)$ is assumed as $T(0)=0.977^3=0.9326$, the transmittance $T(I)$ is plotted as shown in Fig. 13(a).

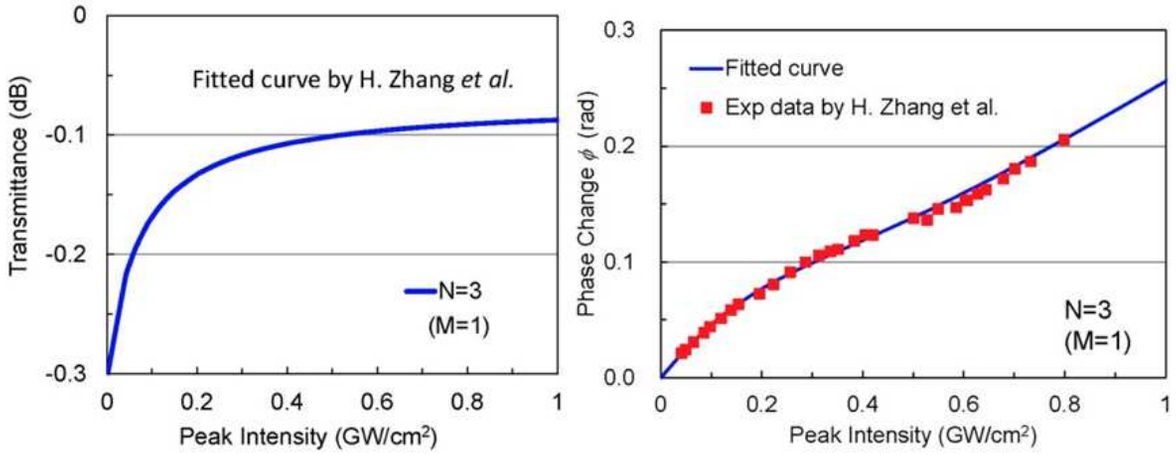

Figure 13. Transmittance and phase change through loosely three-layered graphene.

Reported experimental data of the accompanied phase change are shown in Fig. 13(b) [9]. We find an experimental formula from these data as follows:

$$\phi(I) = k_0 L I\left[a_1 \exp\left(-a_2 I^{a_3}\right) + n_{2,c}\right] \times 10^9 \tag{21}$$

where $k_0=2\pi/\lambda$ with λ=1.55 μm, L =1 nm, and the fitted parameters are $n_{2,c}=6.3\times10^{-8}$ cm^2/W, $a_1=6.75\times10^{-8}$, a_2=6.49, and a_3=1.34. The optical incident peak power density is in unit of GW/cm^2. The fitted curve is also shown in Fig. 13(b). This phase change was derived from

nonlinear refractive index which might include parametric process such as four-wave mixing and strong nonparametric process [9].

We now estimate transmittance T_{3M} and phase change ϕ_{3M} in $3M$-layer graphene. Using $T(I)$ and $\phi(I)$ for three-layer graphene, we can derive $T_{3M}(I)$ by

$$\begin{cases} T_{3M}\left(I_{\text{in}}\right) = T(I_{\text{in}})\prod_{k=1}^{M-1} T(I_{\text{out},k}) \\ I_{\text{out},k} = I_{\text{out},k-1}T\left(I_{\text{out},k-1}\right) \text{ and } I_{\text{out},0} = I_{\text{in}} \end{cases} \tag{22}$$

where I_{in} is the incident optical peak power density. The phase change $\phi_{3M}(I)$ from the phase at I_{in}=0 is given by

$$\phi_{3M}\left(I_{\text{in}}\right) = \sum_{k=0}^{M-1} \phi(I_{\text{out},k}) \tag{23}$$

Fig. 14 shows the transmittance and the phase change, where $N=3M$, It is approximately estimated that the transmittance can be changed by $2K$ dB with $N=30K$, where K = 1,..., 4. Phase change of K rad is accompanied by increasing the peak power density to $0.4 \sim 0.5\ \text{GW}/\text{cm}^2$. From these results, we can estimate the required layer number to satisfy the switching conditions when the graphene is vertically introduced in the waveguide. However, it is noted that the nonlinear phase shift discussed in this section is the phase shift of the incident intense light, that is, not for weak signal light whose wavelength or polarization is different from that of the control light. Therefore, nonlinear phase shift in the proposed switch structure has to be investigated in detail.

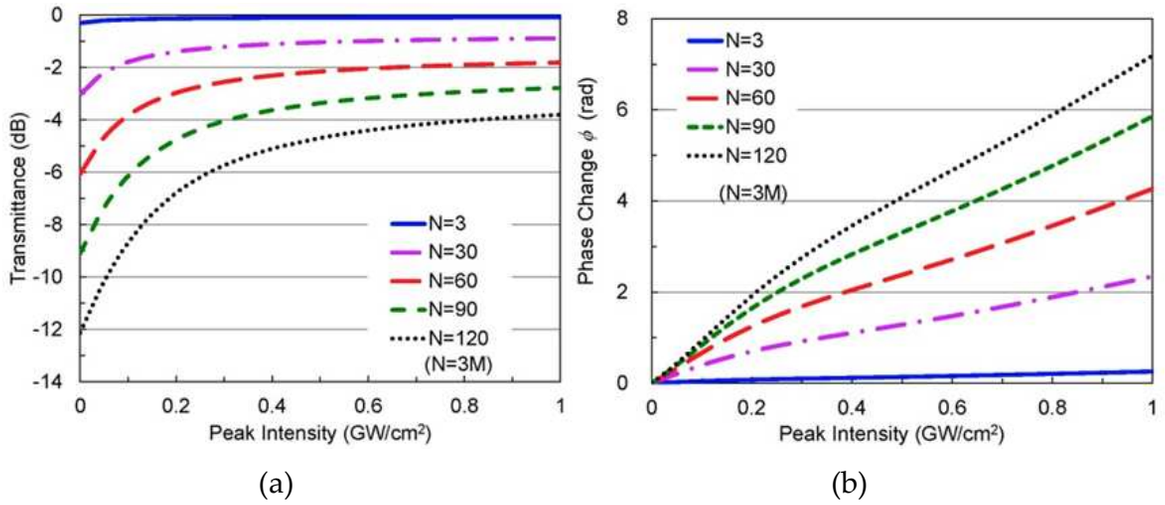

(a) (b)

Figure 14. Transmittance and phase change through loosely multi-layered graphene.

8. Conclusions

Generalized switching conditions for the proposed switch were derived and confirmed by FD-BPM. It is found that the associated refractive-index change can reduce the required absorption decrease in saturable absorption. As a measured saturable absorption, nonlinear insertion loss along graphene-loaded waveguide was discussed. Also, evaluation of nonlinear transmittance and phase shift in multilayered graphene was described. Since conventional switches utilize only phase change to operate switching, the proposed switch, which uses both phase change and absorption change will give a new switching scheme.

Acknowledgements

This work was supported in part by JSPS KAKENHI (23656243 and 24360150).

Author details

Misaki Takahashi, Hiroki Kishikawa, Nobuo Goto * and Shin-ichiro Yanagiya

*Address all correspondence to: goto.nobuo@tokushima-u.ac.jp

Department of Optical Science and Technology, Tokushima University, Tokushima, Japan

References

[1] Doran N. J. and Wood D. Nonlinear-Optic Loop Mirror. *Optics Lett*. 1988, 13(1), 56-58.

[2] Nakamura S., Ueno Y., Tajima K., Sasaki J., Sugimoto T., Kato T., Shimoda T., Itoh M., Hatakeyama H., Tamanuki T., and Sasaki T. Demultiplexing of 168-Gb/s Data Pulses with a Hybrid-Integrated Symmetric Mach-Zehnder All-Optical Switch. *IEEE Photon Tech Lett*. 2000, 12(4), 425-427.

[3] Kitagawa Y., Ozaki N., Takata Y., Ikeda N., Watanabe Y., Sugimoto Y., and Asakawa K. Sequential Operations of Quantum Dot/Photonic Crystal All-Optical Switch With High Repetitive Frequency Pumping. IEEE/OSA *J Lightwave Technol*. 2009, 27(10), 1241-1247.

[4] Kishikawa H., Kimiya K., Goto N., and Yanagiya S. All-Optical Wavelength-Selective Switch Consisting of Asymmetric X-junction Couplers and Raman Amplifiers for Wide Wavelength Range. IEEE/OSA *J of Lightwave Technol*. 2010, 28(1), 172-180.

[5] Kishikawa H., Goto N., and Kimiya K. All-Optical Wavelength-Selective Switch by Intensity Control in Cascaded Interferometers. In *Frontiers in Guided Wave Optics and Optoelectronics*: Bishnu Pal (ed.), Intech; 2010. pp. 257-268.

[6] Oya M., Kishikawa H., Goto N., and Yanagiya S. All-Optical Switch Consisting of Two-Stage Interferometers Controlled by Using Saturable Absorption of Monolayer Graphene. *Opt Express*. 2012, 20(24), 27322-27330.

[7] Takahashi M., Ueda W., Goto N., and Yanagiya S. Saturable Absorption by Vertically Inserted or Overlaid Monolayer Graphene in Optical Waveguide for All-Optical Switching Circuit. *IEEE Photon J*. 2013, 5(5), 6602109.

[8] Takahashi M., Kishikawa H., Goto N., and Yanagiya S. All-Optical Switch with Cascaded Two-Stage Mach-Zehnder Interferometers Using Saturable Absorption Accompanied by Refractive-Index Change in Graphene. *IEEE/OSA J of Lightwave Technol*. 2014, 32(21), 3624-3630.

[9] Zhang H., Virally S., Bao Q., Ping L. K., Massar S., Godbout N., and Kockaert P. Z-scan Measurement of the Nonlinear Refractive Index of Graphene. *Opt Lett*. 2012, 37(11), 1856-1858.

[10] Geim A. K. and Novoselov K. S. The Rise of Graphene. *Natur Mater*. 2007, 6, 183-191.

[11] Iechika, Y. Application of Graphene to High-Speed Transistors: Expectations and Challenges. *Sci Technol Trends Quarter Rev* 2010, 37, 76-92.

[12] Sun Z., Hasan T., Torrisi F., Popa D., Privitera G., Wang F., Bonaccorso F., Basko D. M., and Ferrari A. C. Graphene mode-locked ultrafast laser. *ACS Nano* 2010, 4(2), 803-810.

[13] Bao Q., Zhang H., Ni Z., Wang Y., Polavarapu L., Shen Z., Xu Q.-H., Tang D. and Loh K. P. Monolayer Graphene as a Saturable Absorber in a Mode-Locked Laser. *Nano Res*. 2011, 4(3), 297-307.

[14] Yamashita S. A Tutorial on Nonlinear Photonics Applications of Carbon Nanotube and Graphene. *IEEE/OSA J Lightwave Technol*. 2012, 30(4), 427-447.

[15] Li W., Chen B., Meng C., Fang W., Xiao Y., Li X., Hu Z., Xu Y., Tong L., Wang H., Liu W., Bao J. and Shen Y. R. Ultrafast All-Optical Graphene Modulator. *Nano Lett*. 2014, 14(2), 955-959.

[16] Ferrari A. C., Meyer J. C., Scardaci V., Casiraghi C., Lazzeri M., Mauri F., Piscanec S., Jiang D., Novoselov K. S., Roth S., and Geim A. K. Raman Spectrum of Graphene and Graphene Layers. *Phys Rev* Lett. 2006, 97, 187401-1-4.

IntechOpen